Magnetoencephalography with temporal spread imaging to visualize propagation of epileptic activity

Sumiya Shibata[a,c], Masao Matsuhashi[c], Takeharu Kunieda[a], Yukihiro Yamao[a,c], Rika Inano[a,c], Takayuki Kikuchi[a], Hisaji Imamura[e], Shigetoshi Takaya[c,e], Riki Matsumoto[b], Akio Ikeda[b], Ryosuke Takahashi[e], Tatsuya Mima[c,f], Hidenao Fukuyama[c], Nobuhiro Mikuni[d], Susumu Miyamoto[a]

a. Department of Neurosurgery, Kyoto University Graduate School of Medicine, 54 Shogoin Kawahara-cho, Sakyo-ku, Kyoto, 606-8507, Japan

b. Department of Epilepsy, Movement Disorders and Physiology, Kyoto University Graduate School of Medicine, 54 Shogoin Kawahara-cho, Sakyo-ku, Kyoto, 606-8507, Japan

c. Human Brain Research Center, Kyoto University Graduate School of Medicine, 54 Shogoin Kawahara-cho, Sakyo-ku, Kyoto, 606-8507, Japan

d. Department of Neurosurgery, Sapporo Medical University Graduate School of Medicine, S1 W17, Chuo-ku, Sapporo, Hokkaido, 060-8556, Japan

e. Department of Neurology, Kyoto University Graduate School of Medicine, 54 Shogoin Kawahara-cho, Sakyo-ku, Kyoto, 606-8507, Japan

f. Graduate School of Core Ethics and Frontier Sciences, Ritsumeikan University, 56-1

Toji-in Kitamachi, Kita-ku, Kyoto, 603-8577, Japan

E-mail address

Sumiya Shibata, sshiba@kuhp.kyoto-u.ac.jp

Masao Matsuhashi, matuhasi@kuhp.kyoto-u.ac.jp

Takeharu Kunieda, kuny@kuhp.kyoto-u.ac.jp

Yukihiro Yamao, yyamao@kuhp.kyoto-u.ac.jp

Rika Inano, inan@kuhp.kyoto-u.ac.jp

Takayuki Kikuchi, tkik@kuhp.kyoto-u.ac.jp

Hisaji Imamura, imamurah@kuhp.kyoto-u.ac.jp

Shigetoshi Takaya, shig.t@kuhp.kyoto-u.ac.jp

Riki Matsumoto, matsumot@kuhp.kyoto-u.ac.jp

Akio Ikeda, akio@kuhp.kyoto-u.ac.jp

Ryosuke Takahashi, ryosuket@kuhp.kyoto-u.ac.jp

Tatsuya Mima, t-mima@fc.ritsumei.ac.jp

Hidenao Fukuyama, fukuyama@kuhp.kyoto-u.ac.jp

Nobuhiro Mikuni, mikunin@sapmed.ac.jp

Susumu Miyamoto, miy@kuhp.kyoto-u.ac.jp

Corresponding author:

Masao Matsuhashi

54 Shogoin Kawahara-cho Sakyo-ku, Kyoto, 606-8507, Japan

Tel: +81-75-751-4346

Fax: +81-75-751-3202

E-mail address: matuhasi@kuhp.kyoto-u.ac.jp

Abstract

Objective: We describe temporal spread imaging (TSI) that can identify the spatiotemporal pattern of epileptic activity using Magnetoencephalography (MEG).

Methods: A three-dimensional grid of voxels covering the brain is created. The array-gain minimum-variance spatial filter is applied to an interictal spike to estimate the magnitude of the source and the time (Ta) when the magnitude exceeds a predefined threshold at each voxel. This calculation is performed through all spikes. Each voxel has the mean Ta (<Ta>) and spike number (N_{sp}), which is the number of spikes whose source exceeds the threshold. Then, a random resampling method is used to determine the cutoff value of N_{sp} for the statistically reproducible pattern of the activity. Finally, all the voxels where the source exceeds the threshold reproducibly shown on the MRI with a color scale representing <Ta>.

Results: Four patients with intractable mesial temporal lobe epilepsy (MTLE) were analyzed. In three patients, the common pattern of the overlap between the propagation and the hypometabolism shown by fluorodeoxyglucose-positron emission tomography (FDG-PET) was identified.

Conclusions: TSI can visualize statistically reproducible patterns of the temporal and spatial spread of epileptic activity.

Significance: TSI can assess the statistical significance of the spatiotemporal pattern based on its reproducibility.

Highlights

Our novel method can show the spatiotemporal spread pattern of epileptic activity.

The reproducibility of its propagation pattern can be statistically confirmed.

The pattern was compared with that of FDG-PET hypometabolism in clinical cases.

Keywords: Magnetoencephalography, Magnetic Resonance Imaging, Fluorodeoxyglucose F18, Positron-Emission Tomography, Mesial Temporal Lobe Epilepsy

Abbreviations:

TSI, temporal spread imaging; ECDs, equivalent current dipoles; HPI, head position indicator; PCA, principal component analysis; MSI, magnetic source imaging

1 Introduction

Spencer (2002) presented the concept of epilepsy as a disorder of large neural networks which are connected functionally and structurally (the epileptic network). This suggests that broad regions of brain structures are related to epileptic activity as part of the epileptic network rather than a single localized region of seizure onset. This concept is supported by the evidence that the hypometabolic zone, as detected using fluorodeoxyglucose-positron emission tomography (FDG-PET), is usually larger than the structural lesion and epileptogenic zone and often extends beyond the temporal lobe in intractable temporal lobe epilepsy (TLE) (Savic et al. , 1997) (Arnold et al. , 1996) (Chassoux et al. , 2004) (Dupont et al. , 1998). One hypothesis to explain the mechanism of extra-temporal hypometabolism in TLE is that frequent propagation of epileptic activity to the extra-temporal area may have impaired metabolism as part of the epileptic network. In support of this hypothesis, an animal study reported lesioning of the putative neural pathway prevented the epilepsy-induced hypometabolism in brain regions remote from an epileptic focus (Bruehl et al. , 1998).

The investigation of propagation of epileptic activity can be helpful to understand the epileptic network. While electrocorticography (ECoG) with intracranial electrodes remains the gold standard method to monitor local propagation of epileptic activity, ECoG with intracranial electrodes is limited by spatial sampling and the invasiveness of

neurological procedures. As magnetoencephalography (MEG) is noninvasive and can monitor the entire brain, it is superior to ECoG for investigating propagation of epileptic activity. In addition, high-resolution recordings of cortical function without attenuation or distortion by the skull or other intervening tissue layers below the scalp can be acquired by MEG. This advantage enables good accuracy of MEG to localize the source of epileptic activity (Knowlton, 2008). MEG analysis with a spatial filter approach, which does not assume a single site of generation, can visualize the spatiotemporal evolution of epileptic activity.

In this paper we describe a newly developed method, temporal spread imaging (TSI), that can identify the spatiotemporal pattern of electrophysiological epileptic activity and assess the statistical significance of the pattern based on its reproducibility. First, a three-dimensional (3D) grid of voxels (5 × 5 × 5 mm) covering the whole brain is created for a patient. The array-gain minimum-variance spatial filter (Sekihara and Nagarajan, 2008) is applied to an interictal MEG spike to estimate the magnitude of the source activity as well as the time value, Ta, when the source activity exceeds a predefined threshold for the first time at each voxel. Then, this calculation is performed through all interictal MEG spikes. As a result, each voxel has two values: the mean Ta (<Ta>) and spike number (N_{sp}), which is the number of MEG spikes whose source activity exceeds the threshold value at the voxel. Then, a random resampling method is used to determine the cutoff value of N_{sp}, N, for the statistically reproducible pattern of the source activity. Finally, all the voxels where the source

activity exceeded the threshold more than N times among the analyzed spikes are shown on the patient's MRI with a color scale representing <Ta>. We also present the application of TSI to four clinical interictal MEG data and compares the results with the hypometabolic areas identified by FDG-PET.

2 Methods

This retrospective study was approved by our Institutional Review Board (E2242). The IRB waived the requirement to obtain signed consent form from individual patients because this was a retrospective data review study and personally identifiable information was removed before data analysis.

2.1 Estimation of source activity

After environmental noise reduction by Signal-Space Projection (Tesche et al. , 1995) and a low-pass filter with a cut-off frequency of 100 Hz, epileptic spikes accompanied by no other spike from 1.5 s before the peak of the spike to 1.5 s after the peak are visually identified. Clearly detectable cardiac artifacts are removed by eliminating the components of the signal that corresponded to electrocardiogram using principal component analysis (PCA). The average magnetic field triggered by cardiac (QRS) peaks is calculated in the time range from 0.3 s before to 0.3 s after the peaks. The baseline is set at 0.2–0.3 s before each peak. Then, the main components of the averaged cardiac artifacts are calculated and removed by

PCA. MEG spikes are cut out into 2.0-s epochs (spike segments, a 1.5-s period before the peak time (T_{peak}) of the MEG spike and a 0.5-s period after T_{peak}) (Fig.1(a)). Noisy channels and noisy epochs are excluded from the further analysis.

A 3D grid of voxels (5 × 5 × 5 mm) covering the whole brain is created for a patient. The array-gain minimum-variance spatial filter (Sekihara and Nagarajan, 2008) is applied to each spike segment to estimate the magnitude of the source activity at each voxel based on a single-sphere head model that is fitted to the skull-brain border of the co-registered structural magnetic resonance imaging (MRI):

$$\text{(Eq. 1)}\quad \boldsymbol{w(r)} = \frac{\boldsymbol{R^{-1}}\,\tilde{\boldsymbol{l}}(\boldsymbol{r})}{\left[\tilde{\boldsymbol{l}}^{\mathrm{T}}(\boldsymbol{r})\boldsymbol{R^{-1}}\,\tilde{\boldsymbol{l}}(\boldsymbol{r})\right]}$$

where ***r*** is the source location vector, ***w(r)*** is the weight vector at location ***r***, $\tilde{\boldsymbol{l}}(\boldsymbol{r})$ is the normalized lead-field vector defined as $\tilde{\boldsymbol{l}}(\boldsymbol{r}) = \boldsymbol{l}(\boldsymbol{r})/||\boldsymbol{l}(\boldsymbol{r})||$ with ***l(r)*** being the lead-field vector at location ***r***, and the superscript T indicates the matrix transpose. The data from the entire range of the spike segments are used to calculate the covariance matrix (***R***). Instead of $\boldsymbol{R}^{-1}$, $(\boldsymbol{R} + \varepsilon\boldsymbol{I})^{-1}$ is used to calculate the source, where ***I*** is the unit matrix and ε is the regularization parameter. The regularization parameter is set to $0.1\mathrm{tr}(\boldsymbol{R})/m$, where tr(·) indicates a trace operation applied to a matrix, and m is the number of the sensors. The source subspace dimension is set to two orthogonal components in the tangential plane. The F value of the source activity at every voxel at every time point within the period from −0.2 to 0.5 s relative to T_{peak} (Analysis Window) is calculated as the sum of squares of the two components

as a numerator and the sum of squares from a baseline period of 1.3 s (−1.5 to −0.2 s relative to T_{peak}) as a denominator (Fig.1 (a)) (Dale et al. , 2000).

A time value, Ta (relative to T_{peak}), is assigned to each voxel (Fig.1 (b)), which is the time when the F value exceeded a predefined threshold for the first time in the Analysis Window. This calculation is performed through all spikes. As a result, each voxel has two values: the mean Ta (<Ta>) and spike number (N_{sp}), which is the number of MEG spikes with an F value at the voxel that exceeds the threshold value (Fig.1 (c)).

2.2 Reproducible identification of activated voxels

To define the cutoff value (N) for N_{sp}, a random resampling method is used. 200 repeats of the aforementioned procedure (2.1) are performed using randomly selected 2.0-s segments from the patient's own MEG data, instead of the spike segments. The number of the sampled segments in one repeat is set to the number of the spike segments of the patient. In each repetition, the maximum N_{sp} value of all voxels are calculated. Therefore, 200 random sets produce the distribution of the 200 maximum N_{sp} values. The N value as the greatest 5th percentile of the maximum N_{sp} distribution for all voxels is determined.

2.3 Visualization of reproducibly activated areas on MRI

All voxels with an F value that exceeds the threshold more than N times among the analyzed spikes are shown on the patient's MRI with a color scale representing <Ta>. To visualize the pial surface, a mesh is constructed from T1-weighted anatomical 3D MRI data

using the FreeSurfer ver. 4.5 software suite for processing and analyzing human brain MRI images (http://surfer.nmr.mgh.harvard.edu/) and the color of the surface was assigned to that of the nearest voxel.

3 Results

We applied TSI to spontaneous MEG data in four patients (Table 1) with intractable mesial temporal lobe epilepsy (MTLE) and compared the results with the hypometabolic areas identified by FDG-PET. They met the following criteria: (i) patients with a medical history, seizure semiology, and electrophysiological findings consistent with MTLE; (ii) those who underwent MEG between 2004 and 2010 at Kyoto University Hospital; (iii) those who showed more than 10 interictal spikes by MEG that met the following criteria: (a) equivalent current dipoles (ECDs) of the spikes being located in the temporal lobe on the side of the epileptic focus (the ipsilateral temporal lobe) and (b) no other spike noted for 3.0 s (from 1.5 s before the peak to 1.5 s after the peak); (iv) those who underwent FDG-PET at Kyoto University Hospital.

3.1 MEG data acquisition

The interictal activity was recorded using a whole-head neuromagnetometer with 204 planar gradiometers and 102 magnetometers (Neuromag MEG system; Elekta Neuromag Oy, Helsinki, Finland) at a sampling rate of 1500 Hz (patient 1) or 603 Hz (patients 2–4) and

passband of 0.1–400 Hz (patient 1), 0.1–200 Hz (patients 2-3), or 0.03–200 Hz (patient 4) for at least about 15 min. All patients were in the supine position with eyes closed and were allowed to sleep during the recording. Scalp EEG was simultaneously recorded to complement spike identification by detecting conventional EEG epileptiform activity.

The location of the sensor array with respect to the head was measured using four head position indicator (HPI) coils. The locations of the coils were determined relative to three marker points (the nasion and two pre-auricular points) using a 3D digitizer (Isotrak 3S1002; Polhemus Navigation Sciences, Inc., Colchester, VT, USA) and more than 40 additional points were digitized on the head. Magnetic signals produced by currents led to the coils were measured at the beginning of each session to calculate the position of the head relative to the MEG sensors. The locations of the three markers, HPI coils, and additional points were used to align the MEG and MRI coordinate systems.

3.2 MEG data analysis

MEG data analysis was conducted using an in-house script running on MATLAB (MathWorks, Inc., Natick, MA, USA) and ECD source locations were determined using Elekta Neuromag Data Analysis Software (Elekta Neuromag Oy).

Only the spikes whose ECD sources were localized within the ipsilateral temporal lobe were accepted for the analysis with TSI. Spikes with different origins may have different propagation patterns because the onset areas are different in the first place. Therefore the

spike selection based on the origin could be helpful for preventing the heterogeneity of the analyzed spikes from effecting the statistical evaluation by TSI. Single ECDs were calculated around the peak time by the least square method using a single-sphere head model fitted to the individual patient. A minimum of 27 sensors was used for estimation. If the ECDs were localized in the ipsilateral temporal lobe with a goodness-of-fit of >80 % and confidence volume of <8000 mm^3, these spikes were used for the further analysis.

TSI was applied to these selected spikes using both gradiometers and magnetometers in each patient. We used 8.5 for the threshold of the F value in all patients.

3.3 FDG-PET data acquisition and analysis

Detailed methods of data acquisition are described elsewhere (Takaya et al. , 2006) (Takaya et al. , 2009) (Imamura et al. , 2016). FDG-PET studies were performed using a PET scanner (Advance; General Electric Medical Systems, Milwaukee, WI, USA).

Voxel-wise comparisons were performed using Statistical Parametric Mapping (SPM) 8 software (Wellcome Trust Centre for Neuroimaging, University College London, UK). The FDG-PET images were spatially normalized to our in-house FDG-PET template using affine and nonlinear warping algorithms of SPM 8. The spatially normalized images were then smoothed using an isotropic Gaussian kernel with a full-width at a half maximum of 16 mm. To remove the confounding effects of global FDG uptake, each voxel value was normalized to the total value of the whole brain using proportional scaling.

A two-sample *t*-test was used to identify hypometabolic brain areas of the patients as compared with 18 right-handed healthy subjects (10 men and 8 women; mean age, 31.3 years; age range, 18–47 years) (Imamura et al. , 2016). Cortical regions showing a decrease in glucose metabolism at a voxel-level threshold of $p = 0.001$ (uncorrected) with a cluster extent threshold of 100 voxels were investigated.

3.4 Comparison of TSI and PET findings

For comparison with the findings of TSI, these hypometabolic areas in the standard space were transferred to the individual T1-weighted anatomical space of each patient using Functional MRI of the Brain Software Library (FSL) ver. 5.0 (http://www.fmrib.ox.ac.uk/fsl) in strict accordance with the following procedures. The individual T1-weighted anatomical space was transferred to the Montreal Neurological Institute (MNI) 152 space using affine transformation and nonlinear warping. The hypometabolic areas were then transferred using the inverse transformation of the resulting transformation matrix.

The precise anatomical location was evaluated based on the Harvard–Oxford cortical structural atlas (Table 2; HarvardOxford-cort-maxprob-thr0-2mm.nii.gz, http://www.cma.mgh.harvard.edu/, the Center for Morphometric Analysis, Harvard Medical School, Boston, MA, USA), which has been implemented in FSL. This atlas was transferred using the inverse transformation above mentioned with nearest neighbor interpolation to the individual T1-weighted anatomical space. The cortical segments, which included two or more

voxels of TSI propagation or FDG-PET hypometabolism, were regarded as segments with positive propagation or hypometabolism, respectively.

The kappa (κ) coefficient (Landis and Koch, 1977) was calculated to evaluate the overlap of the propagation pattern of the epileptic activity and the hypometabolic areas in the extra-temporal areas. To do this, we calculated values for Po (the observed degree of concordance) and Pc (the expected chance of concordance). In this study Po was defined as follows:

$$\text{(Eq. 2)}\quad Po = (N_{TSI+PET+} + N_{TSI-PET-})/N_{all},$$

where $N_{TSI+PET+}$ is the number of segments for which both propagation and hypometabolism were identified outside the ipsilateral temporal lobe, $N_{TSI-PET-}$ is the number of the segments for which neither propagation nor hypometabolism was identified outside the ipsilateral temporal lobe, and N_{all} is the number of all segments outside the ipsilateral temporal lobe. Pc was defined as follows:

$$\text{(Eq. 3)}\quad Pc = (N_{TSI+}/N_{all})\,(N_{PET+}/N_{all}) + (N_{TSI-}/N_{all})\,(N_{PET-}/N_{all}),$$

where N_{TSI+} is the number of the segments for which propagation was identified outside the ipsilateral temporal lobe, N_{TSI-} is the number of the segments for which propagation was not identified outside the ipsilateral temporal lobe, N_{PET+} is the number of the segments for which hypometabolism was identified outside the ipsilateral temporal lobe, and N_{PET-} is the number of the segments for which hypometabolism was not identified outside the ipsilateral temporal

lobe. Then, we calculated the κ coefficient according to the following formula:

$$\text{(Eq. 4)}\ \ \kappa = (Po - Pc)/(1 - Pc).$$

The adequacy of the κ coefficient was evaluated using the descriptive ranges of <0, 0.01–0.20, 0.21–0.40, 0.41–0.60, 0.61–0.80, and 0.81–0.99, which are considered to be less than chance concordance, slight concordance, fair concordance, moderate concordance, substantial concordance, and almost perfect concordance, respectively (Viera and Garrett, 2005).

3.5 The results of the comparison

TSI showed that interictal epileptic activity originated from the ipsilateral temporal lobe and then radiated outward in all patients. In 75% patients (patients 1–3), interictal activity spread to the ipsilateral frontal lobe, particularly the ventrolateral prefrontal region. Moreover, hypometabolic areas were identified outside as well as within the ipsilateral temporal lobe, while extra-temporal hypometabolic areas were identified in the ventrolateral prefrontal region ipsilateral to the epileptic focus (patients 1–3), in the contralateral temporal lobe (patient 2), and in the posterior cingulate gyrus (patient 4). In the ventrolateral prefrontal region ipsilateral to the epileptic focus, some of the hypometabolic areas were overlapped with the areas to which interictal epileptic activity had propagated in these three patients.

3.5.1 Patient 1 (Fig. 2, Table 3, and Supplementary Figure 1)

Areas involved in both propagation and hypometabolism were identified in the right frontal orbital cortex, the right insular cortex, the right frontal pole, the right inferior frontal

gyrus pars triangularis, the right supramarginal gyrus posterior division, and the right lateral occipital cortex inferior division. The κ coefficient was 0.37, suggesting fair concordance between these areas.

3.5.2 Patient 2 (Fig. 3, Table 3, and Supplementary Figure 2)

Areas involved in both propagation and hypometabolism were identified in the right frontal pole and the right inferior frontal gyrus pars triangularis. The κ coefficient was 0.10, suggesting slight concordance between these areas.

3.5.3 Patient 3 (Fig. 4, Table 3, and Supplementary Figure 3)

Areas involved in both propagation and hypometabolism were identified in the left frontal pole, the left frontal medial cortex, the left frontal orbital cortex, and the left insular cortex. The κ coefficient was 0.41, suggesting moderate concordance between these areas.

3.5.4 Patient 4 (Fig. 5, Table 3, and Supplementary Figure 4)

Areas involved in both propagation and hypometabolism was identified in the right insular cortex. The κ coefficient was 0.66, suggesting substantial concordance between these areas. Additional extra-temporal hypometabolic areas were identified in the posterior cingulate gyrus (Fig. 5(d)). The cingulate cortices, which are small, irregular, and surrounded by adjacent structures of markedly different pixel values (isotope concentrations), are significantly influenced by the partial volume effect in PET recordings (Mazziotta et al. , 1981). Furthermore, considering that most of the hypometabolic areas were localized within

the ventricle and white matter, rather than within the cortex, the hypometabolism in this area was likely an artifact. When we exclude this area, the κ coefficient would be 1.0, suggesting perfect concordance between propagation and hypometabolism.

4 Discussion

We have described a novel method, TSI, for visualizing the statistically reproducible propagation pattern of epileptic activity. TSI first estimates the spatiotemporal pattern of the source activity for each MEG spike using the spatial filter. It then statistically assesses the reproducibility of the pattern through all MEG spikes using the random resampling method. The statistically reproducible pattern is finally shown on the patient's MRI.

4.1 Advantages of TSI

TSI is a relatively new method to simultaneously analyze the temporal and spatial distribution of epileptic activity and obtain information as to whether the reproducibility is statistically significant in a particular patient. In our previous study, TSI was used to identify the epileptic focus (Matsuhashi et al. , 2012). Although the statistical reproducibility of the epileptic activity could not be monitored by TSI with a random resampling method, that report suggested that TSI might be able to localize the epileptic focus comparable to or better than conventional ECD analysis. In the current study, we analyzed spikes with ECDs that were localized in the ipsilateral temporal lobe. TSI showed that interictal epileptic activity originated from the temporal lobe in all patients. The results of the present study also

determined that TSI was as useful as conventional ECD analysis to identify the epileptic focus.

In addition, TSI can be used to analyze the propagation of the epileptic activity because of the following advantages. First, TSI may be sufficient to estimate the spread of epileptic activity as a function of time and analyze this activity without a designated region of interest. The conventional single ECD model has been demonstrated as an effective method to locate the site of interictal spike generation (Stefan et al. , 2003) (Knowlton et al. , 1997) (Oishi et al. , 2006). However, this model is based on the assumption that interictal epileptiform activity consists of a very small number of focal sources, which is useful to localize the irritative zone and the seizure onset zone of focal epilepsy, as well as to track changes in the irritable area with time as far as it follows this assumption. On the other hand, with this ECD model, it is difficult to monitor the widespread propagation of epileptic activity over certain areas of the brain, while methods that do not require the assumption of a single source are less arbitrary and, thus, more appropriate to describe the extension and dynamics of the activity. TSI employs a spatial filter approach, which does not assume a single site of generation, but rather can visualize the temporal evolution of epileptic activity by analyzing the activity timeline at each source location. Therefore, TSI has advantages over single ECD model when analyzing the extent of epileptic activity.

Second, TSI can identify the tendency of epileptic activity across all MEG spikes in

each patient without averaging signals. Wennberg and Cheyne (2014) used spike averaging to identify the tendency of epileptic activity across multiple MEG spikes in individual patients, as a simple and easy approach applicable to all patients with multiple spikes. However, the signal averaging procedure assumes that the signal of interest is exactly time-locked to an event (for example, a spike peak), which remains invariable across all spikes. Since epileptic activity is variable, even within an individual patient (Alarcon et al. , 1994), the tendency of epileptic activity across multiple MEG spikes is not always representable by an averaged spike with adequate fidelity. This challenge of a variable time course of epileptic activity is solved by applying a spatial filter to each spike in TSI to identify the areas that become active at various latencies relative to T_{peak}. Therefore, TSI can also identify such activity that might be canceled out in the averaged MEG data due to various latencies when the activity is not so strong.

Third, TSI can statistically evaluate the reproducibility of the identified epileptic activity. Past studies have described spatiotemporal analysis of MEG to monitor spike propagation (Shiraishi et al. , 2005a) (Shiraishi et al. , 2005b) (Tanaka et al. , 2010). However, these studies analyzed typical spikes, but did not statistically evaluate the reproducibility of the identified propagation patterns. On the other hand, TSI can define the threshold of the spike number (N_{sp}) at a given family-wise error rate, as estimated by performing a random resampling method. Hence, TSI has the advantage of identifying a statistically reproducible

pattern of spike propagation.

4.2 Electrophysiological Approach to Monitor the Epileptic Network

Halász (2010) reported the use of three electrophysiological factors to monitor the epileptic network: seizure activity, interictal spike occurrence, and high frequency oscillation (HFO). Because the epileptic network is associated with seizure activity, the propagation pattern of ictal discharge may provide valuable information about the epileptic network (Spencer, 2002). Alarcon et al. (1994) showed that the temporal and spatial distribution of interictal discharges arose from the propagation of neuronal activity along neural pathways, while Wang et al. (2012) suggested that pathways of interictal spike propagation was helpful to elucidate the epileptic network underlying focal epilepsy. The results of these studies showed that monitoring of interictal, as well as ictal, discharges was an important approach to clarify the epileptic network. HFO has raised considerable interest as a novel marker of epileptogenicity. However, the underlying mechanisms remain unknown and there is currently no established method to conduct such analysis, as HFO analysis is not a routine clinical procedure (Jacobs et al. , 2012).

In this study, TSI was used to monitor interictal discharges (spikes) to further elucidate the characteristics of the interictal epileptic network. Interictal discharges are usually encountered more often than ictal discharges during recording. Interictal discharges have been the hallmark of epilepsy for quite some time (Pillai and Sperling, 2006). Alarcon et

al. (1994) pointed out that many of the propagation pathways underlying seizure induction coincided with those of interictal discharges in MTLE. Hence, additional analysis of the propagation of interictal discharges is expected to further clarify the epileptic network.

4.3 Comparisons of Propagation to the Extra-temporal Hypometabolic Areas

Comparisons of the findings among different modalities is crucial to elucidate the epileptic network. Magnetic source imaging (MSI), which is a combination of MEG and structural MRI, can noninvasively detect electrophysiological activities in the whole brain with high temporal and spatial resolution. Meanwhile, FDG-PET provides useful information regarding glucose metabolism in the brain. Although the underlying neurobiology of interictal hypometabolism remains unclear (Willmann et al. , 2007), hypometabolism in FDG-PET is reported to reflect the degree of cerebral dysfunction in patients with epilepsy (Rausch et al. , 1994) (McDonald et al. , 2006) (Takaya et al. , 2006). Extra-temporal hypometabolism in patients with TLE represents an chronic impairment of the functional network. Therefore, the combination of MSI and PET may be useful to evaluate the epileptic network from both physiological and functional aspects.

In this study, the propagation patterns varied among the patients, but a certain feature was notable: in each of the current four patients, interictal epileptic activity seemed to radiate from the ipsilateral temporal lobe and then tended to spread to the ipsilateral frontal lobe in three. Because patients with MTLE have many clinical and electrophysiological similarities

(Tatum IV, 2012), they are likely to share characteristic propagation patterns of epileptic activity. Lieb et al. (2007) demonstrated that the ictal epileptic activity in MTLE initiated at the temporal focus and propagated to the ipsilateral frontal lobe, the contralateral frontal lobe, and the contralateral temporal lobe, and found that the ipsilateral frontal lobe, particularly the prefrontal region, was influenced by mesial temporal ictal activity. Moreover, Emerson et al. (1995) demonstrated that the interictal spikes propagated from the anterior temporal region to the posterior temporal region and the frontopolar region. Our findings of the propagation patterns of epileptic activity were consistent with those of these studies although the number of the patients in our study was very small.

Hypometabolic areas beyond the ipsilateral temporal lobe were identified in all four patients in the present study. In three of these four patients, metabolism within the ipsilateral ventrolateral prefrontal region was impaired. Wong et al. (2010) demonstrated that extra-temporal glucose hypometabolism in MTLE was common and frequently occurred in the ipsilateral frontal lobe. Our findings of glucose hypometabolism in the frontal lobe were consistent with this report.

Our results indicated overlapping of the propagation areas with some extra-temporal hypometabolic regions in the ipsilateral ventrolateral prefrontal region (patients 1–3). Intermittent bombardment of subclinical epileptic activity was suggested to lead to interictal glucose hypometabolism outside the focus area (Merlet et al. , 1996). Theodore et al. (2005)

reported metabolic changes within areas with repeated seizure spread and suggested that these changes might be caused by alterations in synaptic organization. Frequent propagation of interictal epileptic activity to the ipsilateral ventrolateral prefrontal regions may have impaired metabolism as part of the epileptic network in MTLE (Takaya et al. , 2006) (Takaya et al. , 2009). The propagation pattern shown by TSI is presumed to represent a chronic network of epileptic activity because the reproducibility of the pattern is statistically evaluated. The hypometabolism in epilepsy patients also partly represents an chronic change due to epileptic activity. Therefore, TSI can fill the gap between electrophysiology and regional glucose metabolism.

4.7 Limitations

We used two thresholds in the TSI analysis: one for the magnitude of source activity and the other one for the extent of activation to delineate the reliable spread pattern. However, TSI was insufficient to monitor interictal spike activity with very low power or rare spread pattern. Therefore, a longer MEG recording with cessation of AEDs might be required to overcome this limitation.

In this study, only TSI was used to monitor MEG spikes. Propagation of interictal epileptic activity could not be monitored in cases with absent or rare interictal MEG spikes. Nonetheless, TSI can be used to slow waves as well as to spikes. Past studies showed that some types of low frequency neuromagnetic activity was useful for localization of an

epileptogenic region (Gallen et al. , 1997) (Ishibashi et al. , 2002). The application of TSI to such slow waves can be useful to investigate the epileptic network in low frequency bands, particularly when interictal MEG spikes are absent or rare.

We could not rule out the possibility that interictal FDG-PET revealed complex patterns of local cerebral glucose utilization. Chugani et al. (1993) revealed that hypermetabolism was interictally observed due to frequent spike activity. Therefore, the metabolic state of the epileptic focus could fluctuate between hypermetabolism and hypometabolism, which could partly explain why some parts of the propagation areas were not involved in remote extra-temporal hypometabolic regions.

5 Conclusions

Although there were some limitations to this study, TSI enabled us to statistically evaluate the reproducibility of the identified epileptic activity and visualize its spatiotemporal spread. The propagation pattern shown by TSI was partly consistent with the hypometabolic areas identified by FDG-PET. TSI can be a useful and non-invasive tool to investigate the epileptic network and to fill the gap between electrophysiology and regional glucose metabolism.

Acknowledgements

This work was supported by Grants-in-Aid for Scientific Research (KAKENHI) (C) from the Ministry of Education, Culture, Sports, Science and Technology of Japan (grant nos.: 24592159, 15K10361) and a Health and Labor Sciences Research Grant for the Comprehensive Research on Disability, Health and Welfare from the Ministry of Health, Labor and Welfare, Japan (grant no.: H21-023). This work was partly supported by Grants-in-Aid for Scientific Research (KAKENHI) (B) (grant nos.: 15H03044), Grants-in-Aid for Scientific Research (KAKENHI) (C) (grant nos.: 26330175), Grants-in-Aid for Scientific Research (KAKENHI) on Innovative Areas (grant nos.: 15H05871, 15H05874, 15H05875, 15H05880) from the Ministry of Education, Culture, Sports, Science and Technology of Japan, the research grant (grant nos.: 27280201, 2736040) from Japan Agency for Medical Research and Development (AMED) and the research grant (2015) from the Brain Science Foundation.

Department of Epilepsy, Movement Disorders and Physiology, Kyoto University Graduate School of Medicine is an endowment department, supported with grants by GlaxoSmithKline K.K., NIHON KOHDEN CORPORATION, Otsuka Pharmaceutical Co., and UCB Japan Co., Ltd.

Disclosure

None of the authors have potential conflicts of interest to be disclosed.

References

Alarcon G, Guy C, Binnie C, Walker S, Elwes R, Polkey C. Intracerebral propagation of interictal activity in partial epilepsy: implications for source localisation. J Neurol Neurosurg Psychiatry. 1994;57:435-49.

Arnold S, Schlaug G, Niemann H, Ebner A, Luders H, Witte O, et al. Topography of interictal glucose hypometabolism in unilateral mesiotemporal epilepsy. Neurology. 1996;46:1422-30.

Bruehl C, Wagner U, Huston J, Witte O. Thalamocortical circuits causing remote hypometabolism during focal interictal epilepsy. Epilepsy Res. 1998;32:379-87.

Chassoux F, Semah F, Bouilleret V, Landre E, Devaux B, Turak B, et al. Metabolic changes and electro-clinical patterns in mesio-temporal lobe epilepsy: a correlative study. Brain. 2004;127:164-74.

Chugani HT, Shewmon DA, Khanna S, Phelps ME. Interictal and postictal focal hypermetabolism on positron emission tomography. Pediatr Neurol. 1993;9:10-5.

Dale AM, Liu AK, Fischl BR, Buckner RL, Belliveau JW, Lewine JD, et al. Dynamic statistical parametric mapping: combining fMRI and MEG for high-resolution imaging of cortical activity. Neuron. 2000;26:55-67.

Dupont S, Semah F, Baulac M, Samson Y. The underlying pathophysiology of ictal dystonia in temporal lobe epilepsy An FDG-PET study. Neurology. 1998;51:1289-92.

Emerson RG, Turner CA, Pedley TA, Walczak TS, Forgione M. Propagation patterns of

temporal spikes. Electroencephalogr Clin Neurophysiol. 1995;94:338-48.

Engel J Jr, Van Ness PC, Rasmussen TB, Ojemann LM. Outcome with respect to epileptic seizures. In: Engel J Jr, editor. Surgical treatment of the epilepsies. New York: Raven Press; 1993. p. 609-21.

Gallen C, Tecoma E, Iragui V, Sobel D, Schwartz B, Bloom F. Magnetic Source Imaging of Abnormal Low-Frequency Magnetic Activity in Presurgical Evaluations of Epilepsy. Epilepsia. 1997;38:452-60.

Halász P. The concept of epileptic networks. Part 1. Ideggyogy szle. 2010;63:293-303.

Imamura H, Matsumoto R, Takaya S, Nakagawa T, Shimotake A, Kikuchi T, et al. Network specific change in white matter integrity in mesial temporal lobe epilepsy. Epilepsy Res. 2016;120:65-72.

Ishibashi H, Simos PG, Castillo EM, Maggio WW, Wheless JW, Kim HL, et al. Detection and significance of focal, interictal, slow-wave activity visualized by magnetoencephalography for localization of a primary epileptogenic region. J Neurosurg. 2002;96:724-30.

Jacobs J, Staba R, Asano E, Otsubo H, Wu J, Zijlmans M, et al. High-frequency oscillations (HFOs) in clinical epilepsy. Prog Neurobiol. 2012;98:302-15.

Knowlton R, Laxer K, Aminoff M, Roberts T, Wong S, Rowley H. Magnetoencephalography in partial epilepsy: clinical yield and localization accuracy. Ann Neurol. 1997;42:622-31.

Knowlton RC. Can magnetoencephalography aid epilepsy surgery? Epilepsy Currents. 2008;8:1-5.

Landis JR, Koch GG. The measurement of observer agreement for categorical data. Biometrics. 1977;33:159-74.

Lieb JP, Dasheiff RM, Engel J. Role of the frontal lobes in the propagation of mesial temporal lobe seizures. Epilepsia. 2007;32:822-37.

Matsuhashi M, Mima T, Fukuyama H, Matsumoto R, Kobayashi K, Ikeda A, et al. Temporal Spread Image to delineate MEG spike foci in epilepsy patients. Complex Medical Engineering (CME), 2012 ICME International Conference on: IEEE; 2012. p. 221-4.

Mazziotta JC, Phelps ME, Plummer D, Kuhl DE. Quantitation in Positron Emission Computed Tomography: 5. Physical-Anatomical Effects. J Comput Assist Tomogr. 1981;5:734-43.

McDonald CR, Swartz BE, Halgren E, Patell A, Daimes R, Mandelkern M. The relationship of regional frontal hypometabolism to executive function: a resting fluorodeoxyglucose PET study of patients with epilepsy and healthy controls. Epilepsy & Behav. 2006;9:58-67.

Merlet I, Garcia–Larrea L, Gregoire M, Lavenne F, Mauguiere F. Source propagation of interictal spikes in temporal lobe epilepsy Correlations between spike dipole modelling and [18F] fluorodeoxyglucose PET data. Brain. 1996;119:377-92.

Oishi M, Kameyama S, Masuda H, Tohyama J, Kanazawa O, Sasagawa M, et al. Single and

multiple clusters of magnetoencephalographic dipoles in neocortical epilepsy: significance in characterizing the epileptogenic zone. Epilepsia. 2006;47:355-64.

Pillai J, Sperling MR. Interictal EEG and the diagnosis of epilepsy. Epilepsia. 2006;47:14-22.

Rausch R, Henry TR, Ary CM, Engel J, Mazziotta J. Asymmetric interictal glucose hypometabolism and cognitive performance in epileptic patients. Arch Neurol. 1994;51:139-44.

Savic I, Altshuler L, Baxter L, Engel J. Pattern of interictal hypometabolism in PET scans with fludeoxyglucose F 18 reflects prior seizure types in patients with mesial temporal lobe seizures. Arch Neurol. 1997;54:129-36.

Sekihara K, Nagarajan SS. Adaptive spatial filters. In: Adaptive spatial filters for electromagnetic brain imaging. Berlin: Springer-Verlag; 2008. p. 37-63.

Shiraishi H, Ahlfors SP, Stufflebeam SM, Takano K, Okajima M, Knake S, et al. Application of Magnetoencephalography in Epilepsy Patients with Widespread Spike or Slow-wave Activity. Epilepsia. 2005a;46:1264-72.

Shiraishi H, Stufflebeam SM, Knake S, Ahlfors SP, Sudo A, Asahina N, et al. Dynamic statistical parametric mapping for analyzing the magnetoencephalographic epileptiform activity in patients with epilepsy. J Child Neurol. 2005b;20:363-9.

Spencer SS. Neural networks in human epilepsy: evidence of and implications for treatment. Epilepsia. 2002;43:219-27.

Stefan H, Hummel C, Scheler G, Genow A, Druschky K, Tilz C, et al. Magnetic brain source imaging of focal epileptic activity: a synopsis of 455 cases. Brain. 2003;126:2396-405.

Takaya S, Hanakawa T, Hashikawa K, Ikeda A, Sawamoto N, Nagamine T, et al. Prefrontal hypofunction in patients with intractable mesial temporal lobe epilepsy. Neurology. 2006;67:1674-6.

Takaya S, Mikuni N, Mitsueda T, Satow T, Taki J, Kinoshita M, et al. Improved cerebral function in mesial temporal lobe epilepsy after subtemporal amygdalohippocampectomy. Brain. 2009;132:185-94.

Tanaka N, Hämäläinen MS, Ahlfors SP, Liu H, Madsen JR, Bourgeois BF, et al. Propagation of epileptic spikes reconstructed from spatiotemporal magnetoencephalographic and electroencephalographic source analysis. Neuroimage. 2010;50:217-22.

Tatum IV WO. Mesial temporal lobe epilepsy. J Clin Neurophysiol. 2012;29:356-65.

Tesche C, Uusitalo M, Ilmoniemi R, Huotilainen M, Kajola M, Salonen O. Signal-space projections of MEG data characterize both distributed and well-localized neuronal sources. Electroencephalogr Clin Neurophysiol. 1995;95:189-200.

Theodore WH, Sato S, Kufta CV, Gaillard WD, Kelley K. FDG-Positron Emission Tomography and Invasive EEG: Seizure Focus Detection and Surgical Outcome. Epilepsia. 2005;38:81-6.

Viera AJ, Garrett JM. Understanding interobserver agreement: the kappa statistic. Fam Med.

2005;37:360-3.

Wang ZI, Jin K, Kakisaka Y, Mosher JC, Bingaman WE, Kotagal P, et al. Imag (in) ing seizure propagation: MEG-guided interpretation of epileptic activity from a deep source. Hum Brain Mapp. 2012;33:2797-801.

Wennberg R, Cheyne D. Reliability of MEG source imaging of anterior temporal spikes: analysis of an intracranially characterized spike focus. Clin Neurophysiol. 2014;125:903-18.

Willmann O, Wennberg R, May T, Woermann F, Pohlmann-Eden B. The contribution of 18F-FDG PET in preoperative epilepsy surgery evaluation for patients with temporal lobe epilepsy A meta-analysis. Seizure. 2007;16:509.

Wong CH, Bleasel A, Wen L, Eberl S, Byth K, Fulham M, et al. The topography and significance of extratemporal hypometabolism in refractory mesial temporal lobe epilepsy examined by FDG-PET. Epilepsia. 2010;51:1365-73.

Figure captions

Figure 1 Analysis by TSI.

(a) MEG waveforms of “Spike Segment”. The MEG spikes were cut to 2.0-s epochs (Spike Segment. 1.5-s period before a peak of the MEG spike (T_{peak}) and 0.5-s period after T_{peak}). F value from the source activity at every time and every voxel using 1.3-s epoch (−1.5 to −0.2 s relative to T_{peak}) as a denominator was calculated.

(b) F value in a voxel. A time value, Ta (which was relative to T_{peak}), when the F value exceeded a predefined threshold (we used 8.5 in this study) for the first time in the “Analysis Window” was given to each voxel.

(c) The mean Ta (<Ta>) and the “Spike Number” (N_{sp}). The Figure shows each voxel has <Ta> (the value on the left side) and N_{sp} (the value on the right side) which is the number of the MEG spikes whose F value at the voxel exceeds the threshold (<Ta>/N_{sp}). The voxels where the power exceeds the threshold above the cutoff value for N_{sp} (N) through the analyzed spikes are shown on the patient’s MRI by the color scale representing <Ta>. For example, if N is 12, the colored voxels are shown.

Figure 2 The propagation and the hypometabolic areas in patient 1.

(a) The propagation pattern on the patient’s 3D MRI. The color scale represented <Ta>.

(b) The hypometabolic areas on the patient’s 3D MRI. Brain regions showing a decrease in glucose metabolism were indicated by magenta color.

(c) The propagation pattern on the patient's axial MRI slices (the left column). The color scale represented <Ta>. The hypometabolic areas on the patient's axial MRI slices (the right column). Brain regions showing a decrease in glucose metabolism were indicated by magenta color. Lt: left.

Both the propagation and the hypometabolism were identified in the right frontal orbital cortex, the right insular cortex, the right frontal pole, the right inferior frontal gyrus pars triangularis, the supramarginal gyrus posterior division and the right lateral occipital cortex inferior division.

Figure 3 The propagation and the hypometabolic areas in patient 2.

(a) The propagation pattern on the patient's 3D MRI. The color scale represented <Ta>.

(b) The propagation pattern on the patient's axial MRI slices (the left column). The color scale represented <Ta>. The hypometabolic areas on the patient's axial MRI slices (the right column). Brain regions showing a decrease in glucose metabolism were indicated by magenta color. Lt: left.

Both the propagation and the hypometabolism were identified in the right frontal pole and the right inferior frontal gyrus pars triangularis.

Figure 4 The propagation and the hypometabolic areas in patient 3.

(a) The propagation pattern on the patient's 3D MRI. The color scale represented <Ta>.

(b) The hypometabolic areas on the patient's 3D MRI. Brain regions showing a decrease in glucose metabolism were indicated by magenta color.

(c) The propagation pattern on the patient's axial MRI slices (the left column). The color scale represented <Ta>. The hypometabolic areas on the patient's axial MRI slices (the right column). Brain regions showing a decrease in glucose metabolism were indicated by magenta color. Lt: left.

Both the propagation and the hypometabolism were identified in the left frontal pole, the left frontal medial cortex, the left frontal orbital cortex and the left insular cortex.

Figure 5 The propagation and the hypometabolic areas in patient 4.

(a) The propagation pattern on the patient's 3D MRI. The color scale represented <Ta>.

(b) The hypometabolic areas on the patient's 3D MRI. Brain regions showing a decrease in glucose metabolism were indicated by magenta color.

(c) The propagation pattern on the patient's axial MRI slices (the left column). The color scale represented <Ta>. The hypometabolic areas on the patient's axial MRI slices (the right column). Brain regions showing a decrease in glucose metabolism were indicated by magenta color. Lt: left.

(d) The hypometabolic areas on the patient's axial MRI slices. Brain regions showing

decreases in glucose metabolism were indicated by magenta color. Most of them were identified within the ventricle and white matter.

The overlap between the propagation and the hypometabolism was identified in the right insular cortex. The interictal epileptic activity did not propagate to the ipsilateral frontal lobe.

Supplementary Figure 1–4 The detailed anatomical map of the hypometabolic areas in patient 1–4 respectively. Brain regions showing a decrease in glucose metabolism were indicated by magenta and other colors according to the segmentations of the Harvard–Oxford cortical structural atlas. The magenta areas included the ipsilateral temporal lobe, the left middle frontal gyrus and the areas which did not correspond to a segmentation of the atlas..

1 (a) The green area, the red area, and the yellow area were classified into the right inferior frontal gyrus pars triangularis, the right frontal pole, and the right frontal orbital cortex respectively.

(b) The green area was classified into the right insular cortex.

(c) The blue area was classified into the right supramarginal gyrus posterior division.

(d) The green area was classified into the right lateral occipital cortex inferior division.

2 The green area and the red area were classified into the right inferior frontal gyrus pars triangularis and the right frontal pole respectively.

3 (a) The blue area and the red area were classified into the left frontal medial cortex and the left frontal pole respectively.

(b) The green area, the red area, and the yellow area were classified into the left insular cortex, the left frontal pole, and the left frontal orbital cortex respectively.

4 The green area was classified into the right insular cortex.

Table 1 Patient profile.

Patient	1	2	3	4
Age/Sex	24/M	27/M	25/F	23/M
Age at Sz onset (years)	12	4	12	12
Sz frequency (average) at the examination of MEG	1–2/w	12–24/m	1–2/w	1–2/m
MRI	Rt HS	Rt HS	Blurred layer of Rt hippocampus	Rt HS
	Enlargement of Rt amygdala		Hyperintensity signal in Lt amygdala	Atrophy of Rt amygdala
AED at the examination of MEG	PHT, VPA, GBP	CBZ, VPA, CLB	PHT, GBP, AZA, NZP	PHT, PB, CLB
Side of the focus	Rt	Rt	Lt	Rt
Age at surgery (years)	24	27	-[a]	23
Surgery	Rt SAH and focus resection	Rt SAH and focus resection	-	Rt SAH
Surgical outcome (Engel classification[b])	IIa	Ib	-	Ia
Number of analyzed MEG spikes	28	20	17	58

[a] Patient 3 did not have surgery.

[b] (Engel Jr, 1993)

w: week, m: month, Rt: right, Lt: left, HS: hippocampal screlosis, AED: antiepileptic drug, PHT: phenytoin, CBZ: carbamazepine, VPA: valproic acid, GBP: gabapentin, PB: phenobarbital, CLB: clobazam, AZA: acetazolamide, NZP: nitrazepam, SAH: selective amygdalohippocampectomy, Sz: seizure

Table 2 The cortical segments of Harvard–Oxford atlas.

No.	Cortical structures
1	Frontal Pole
2	Insular Cortex
3	Superior Frontal Gyrus
4	Middle Frontal Gyrus
5	Inferior Frontal Gyrus, pars triangularis
6	Inferior Frontal Gyrus, pars opercularis
7	Precentral Gyrus
8	Temporal Pole *
9	Superior Temporal Gyrus, anterior division *
10	Superior Temporal Gyrus, posterior division *
11	Middle Temporal Gyrus, anterior division *
12	Middle Temporal Gyrus, posterior division *
13	Middle Temporal Gyrus, temporooccipital part *
14	Inferior Temporal Gyrus, anterior division *
15	Inferior Temporal Gyrus, posterior division *
16	Inferior Temporal Gyrus, temporooccipital part *
17	Postcentral Gyrus
18	Superior Parietal Lobule
19	Supramarginal Gyrus, anterior division
20	Supramarginal Gyrus, posterior division
21	Angular Gyrus
22	Lateral Occipital Cortex, superior division
23	Lateral Occipital Cortex, inferior division
24	Intracalcarine Cortex
25	Frontal Medial Cortex
26	Juxtapositional Lobule Cortex (supplementary motor cortex)
27	Subcallosal Cortex
28	Paracingulate Gyrus
29	Cingulate Gyrus, anterior division
30	Cingulate Gyrus, posterior division
31	Precuneus Cortex
32	Cuneal Cortex
33	Frontal Orbital Cortex
34	Parahippocampal Gyrus, anterior division *
35	Parahippocampal Gyrus, posterior division *

36 Lingual Gyrus
37 Temporal Fusiform Cortex, anterior division *
38 Temporal Fusiform Cortex, posterior division *
39 Temporal Occipital Fusiform Cortex *
40 Occipital Fusiform Gyrus
41 Frontal Operculum Cortex
42 Central Opercular Cortex
43 Parietal Operculum Cortex
44 Planum Polare *
45 Heschl's Gyrus (includes H1 and H2) *
46 Planum Temporale *
47 Supracalcarine Cortex
48 Occipital Pole

* These segments were defined as the segments inside the temporal lobe.

Table 3 The time when the interictal activity propagated to the extra-temporal cortical segments. It is the relative time with reference to $T_{peak.}$

Patient 1

	Segment	Time (ms)	Hypometabolism
Rt	Lingual Gyrus	−50	
Rt	Cingulate Gyrus, posterior division	−37	
Rt	Subcallosal Cortex	−35	
Rt	Frontal Orbital Cortex	−35	*
Rt	Insular Cortex	−27	*
Rt	Central Opercular Cortex	−26	
Rt	Frontal Pole	−23	*
Rt	Parietal Operculum Cortex	−18	
Rt	Inferior Frontal Gyrus, pars triangularis	−16	*
Rt	Frontal Operculum Cortex	−7	
Rt	Postcentral Gyrus	−5	
Rt	Supramarginal Gyrus, anterior division	−5	
Rt	Inferior Frontal Gyrus, pars opercularis	4	
Rt	Precentral Gyrus	5	
Rt	Precuneus Cortex	12	
Rt	Cingulate Gyrus, anterior division	14	
Rt	Supramarginal Gyrus, posterior division	15	*
Rt	Frontal Medial Cortex	23	
Rt	Lateral Occipital Cortex, inferior division	36	*
Rt	Occipital Fusiform Gyrus	46	
Rt	Paracingulate Gyrus	47	

Patient 2

	Segment	Time (ms)	Hypometabolism
Rt	Frontal Pole	−29	*
Rt	Frontal Orbital Cortex	−25	
Rt	Frontal Operculum Cortex	−14	
Rt	Insular Cortex	−14	
Rt	Inferior Frontal Gyrus, pars triangularis	−4	*
Rt	Inferior Frontal Gyrus, pars opercularis	8	

Patient 3

	Segment	Time (ms)	Hypometabolism
Lt	Frontal Pole	−37	*
Lt	Frontal Medial Cortex	−37	*
Lt	Frontal Orbital Cortex	−19	*
Lt	Insular Cortex	−16	*
Lt	Paracingulate Gyrus	−10	
Lt	Cingulate Gyrus, anterior division	−10	
Lt	Cingulate Gyrus, posterior division	−5	
Lt	Subcallosal Cortex	−2	
Rt	Subcallosal Cortex	22	
Rt	Frontal Medial Cortex	23	

Patient 4

	Segment	Time (ms)	Hypometabolism
Rt	Insular Cortex	−20	*

* The segments where the hypometabolic areas were identified.

Rt: right, Lt: left

(a)

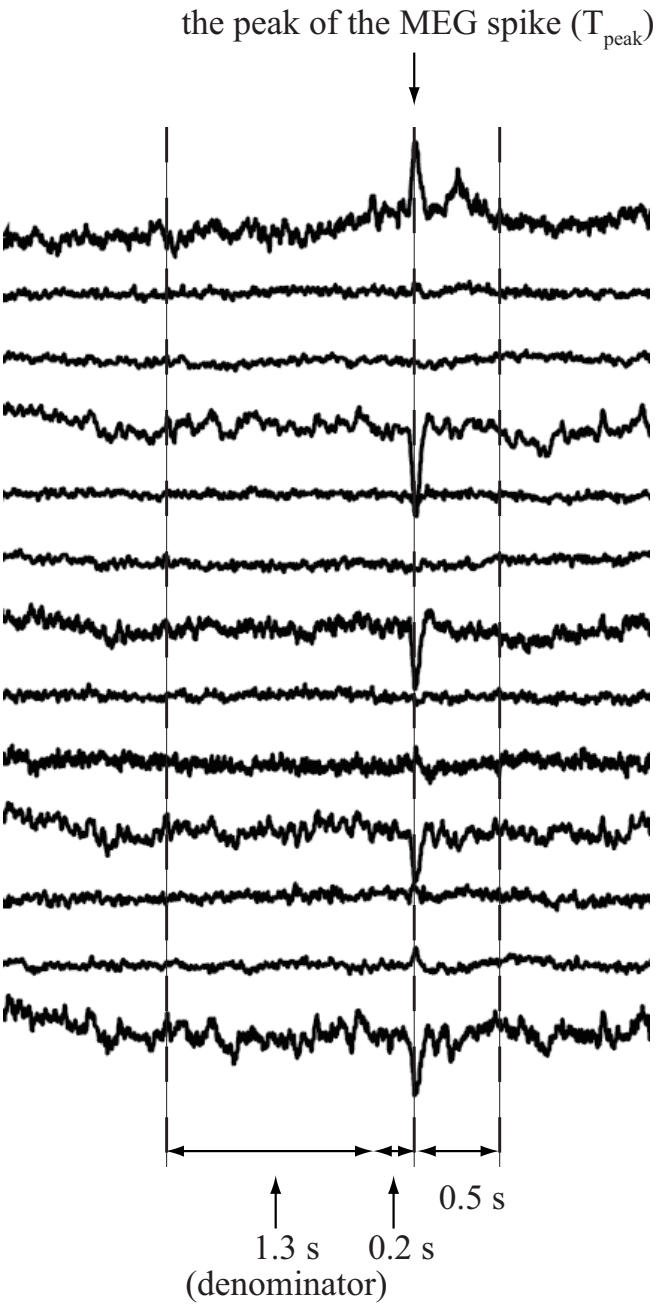

(b)

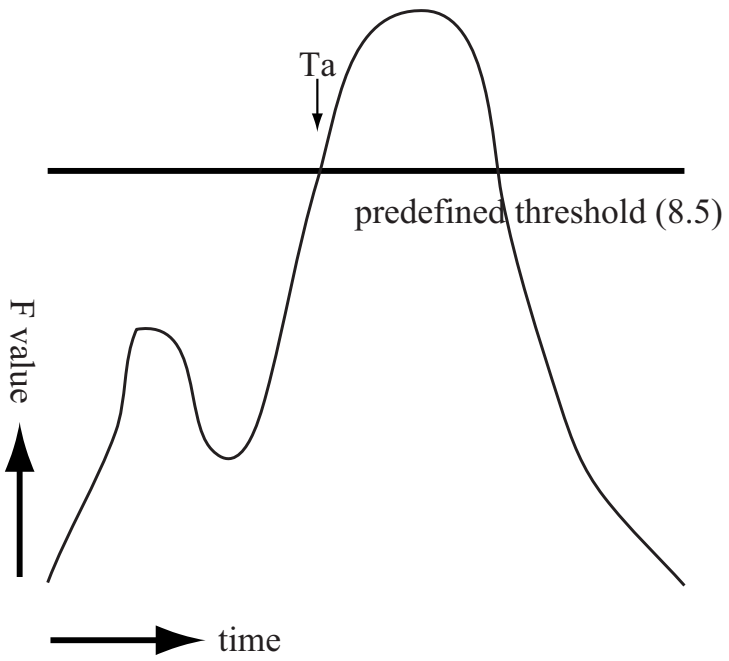

(c)

	−33/13	−32/16	−32/10	−33/8	−31/10	
	−31/14	−20/15	−24/15	−20/17	−15/10	
	−20/14	−15/16	−23/13	−32/9	−26/16	
	−25/9	−30/13	−29/16	−30/14	−30/13	

Fig. 1

(a)

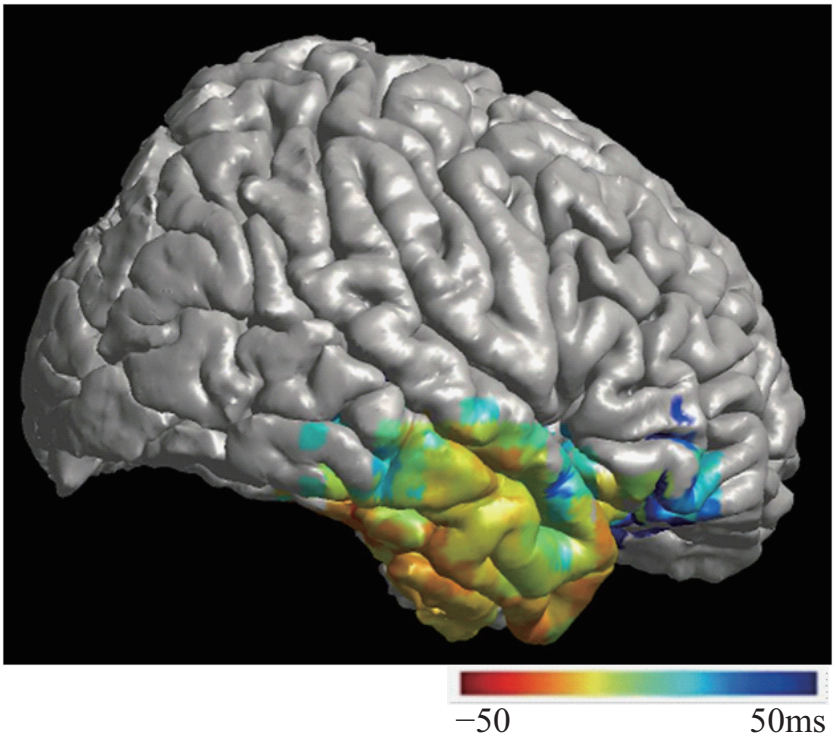

−50 50ms

(b)

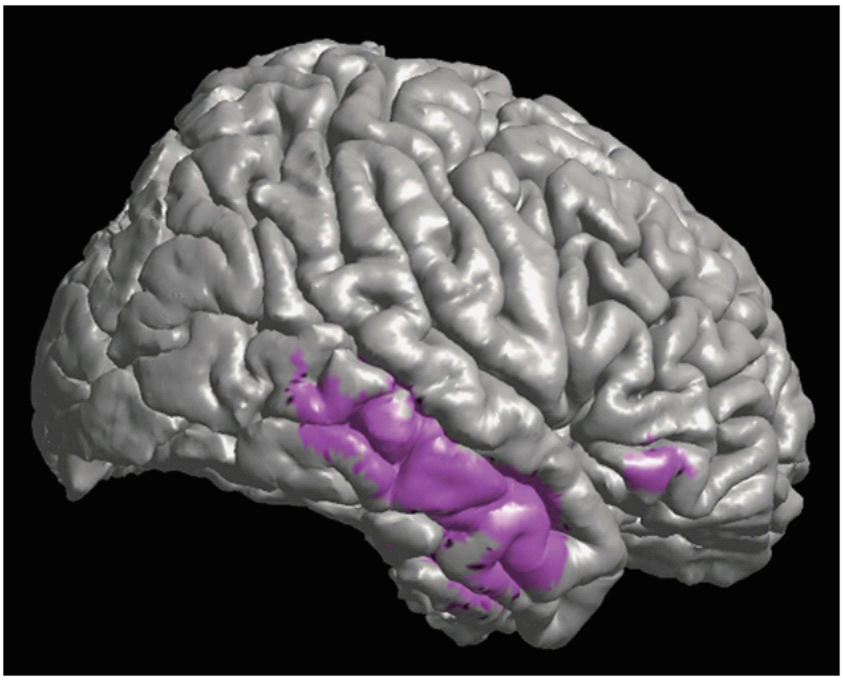

(c)

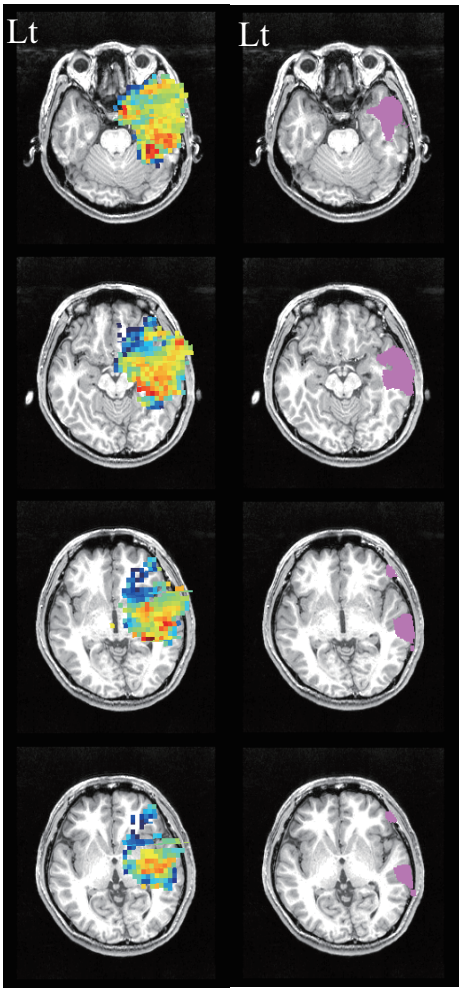

−50 50ms

Fig. 2

(a)

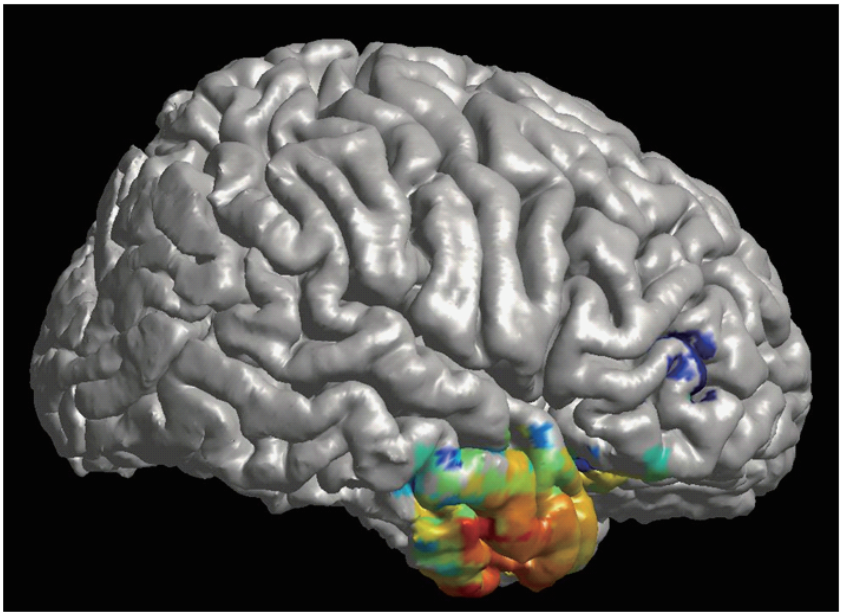

−50 50ms

(b)

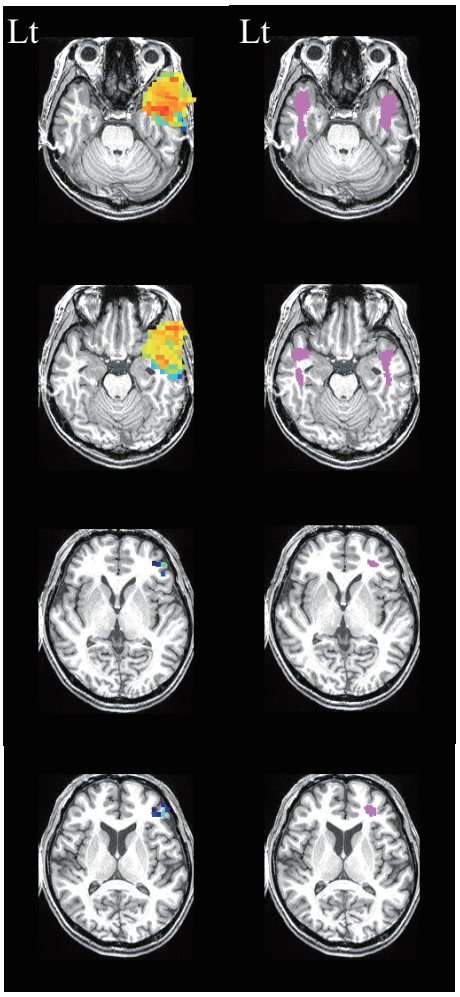

−50 50ms

Fig. 3

(a)

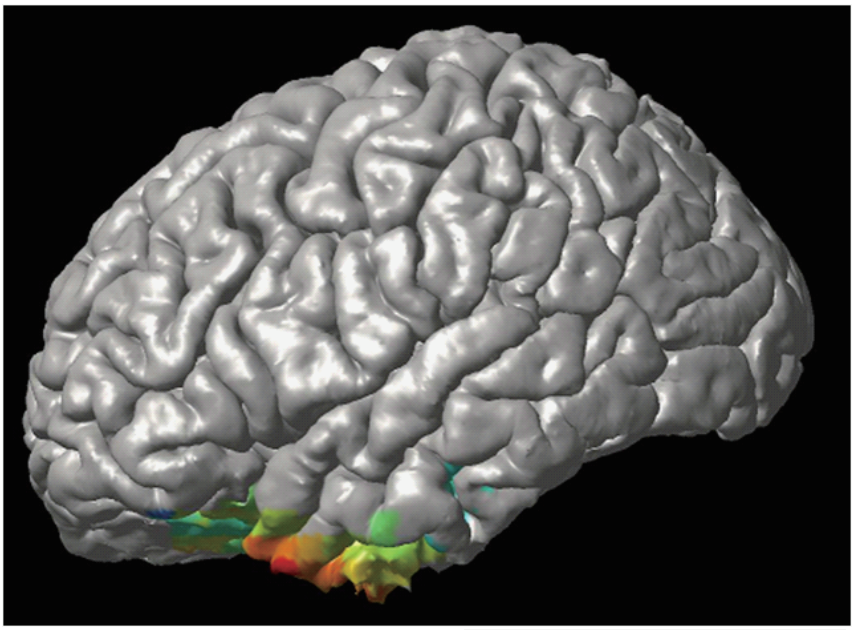

−50 50ms

(b)

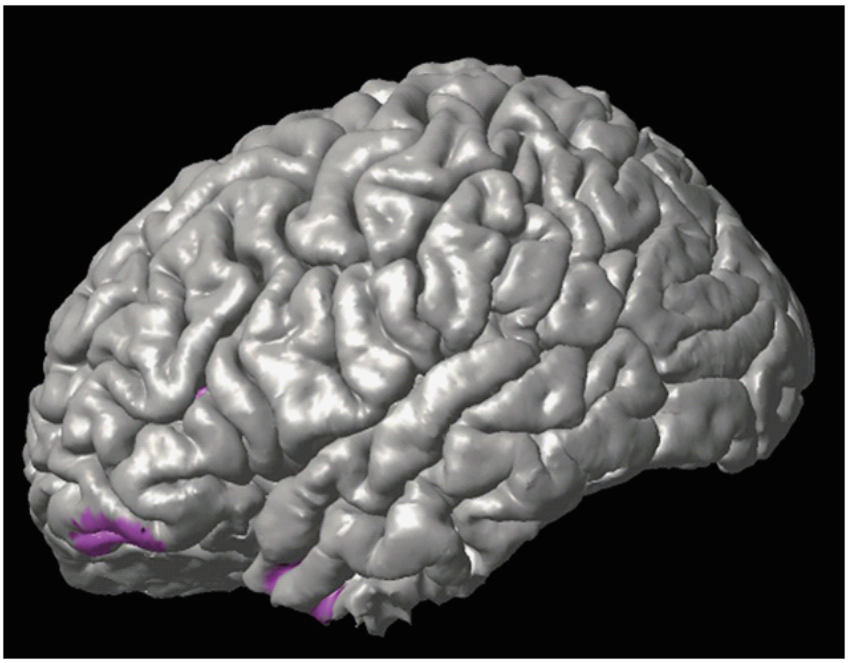

(c)

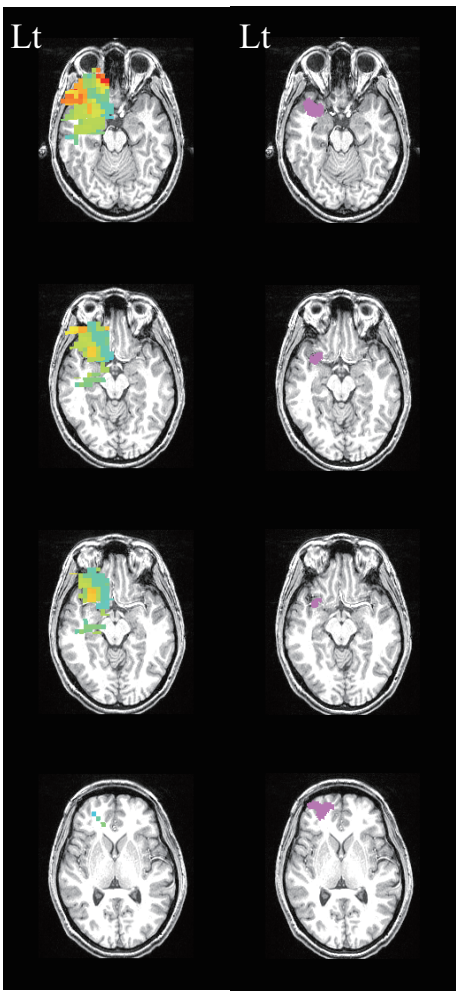

−50 50ms

Fig. 4

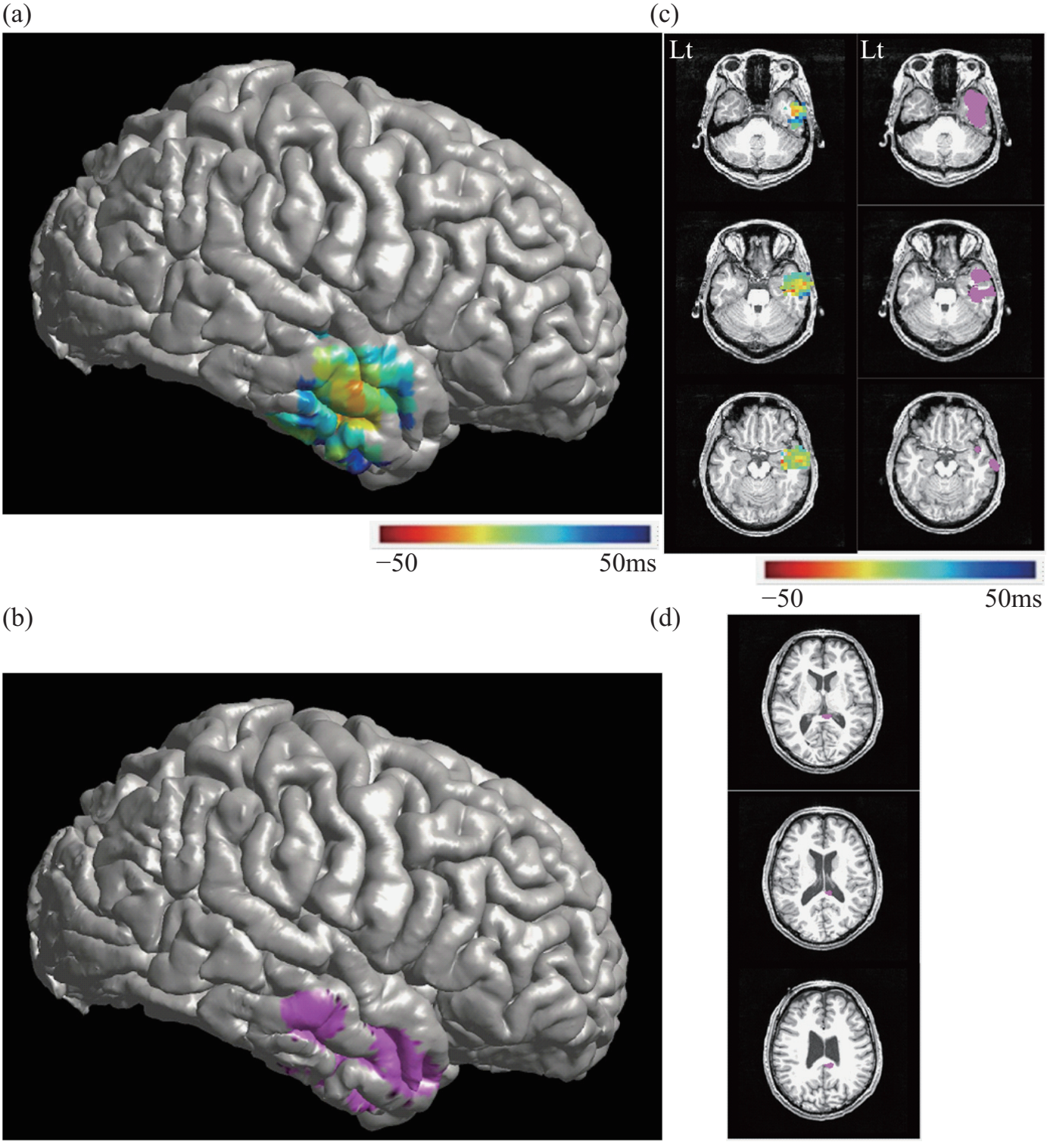

Fig. 5

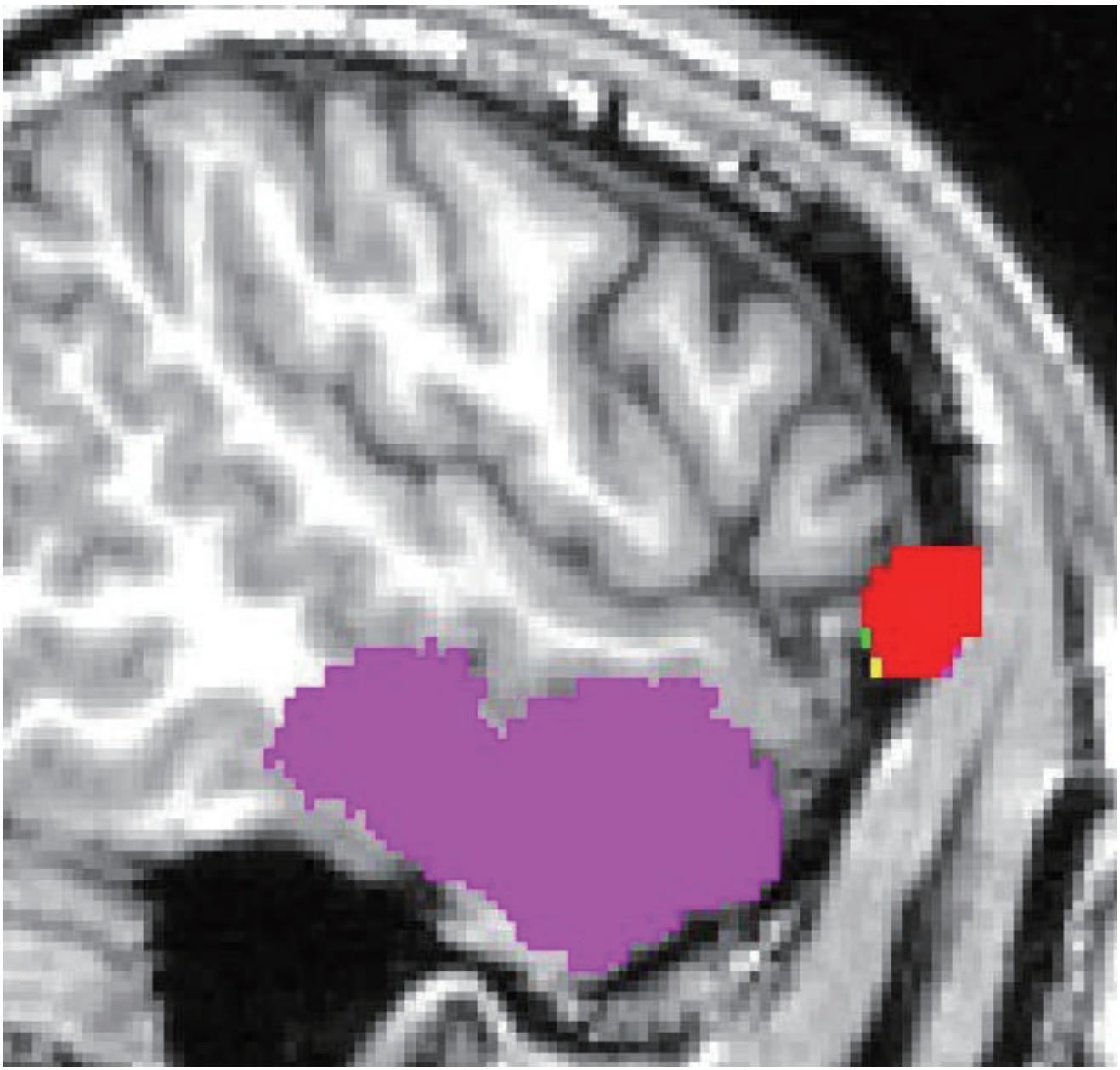

Supplementary Fig. 1(a)

Supplementary Fig. 1(b)

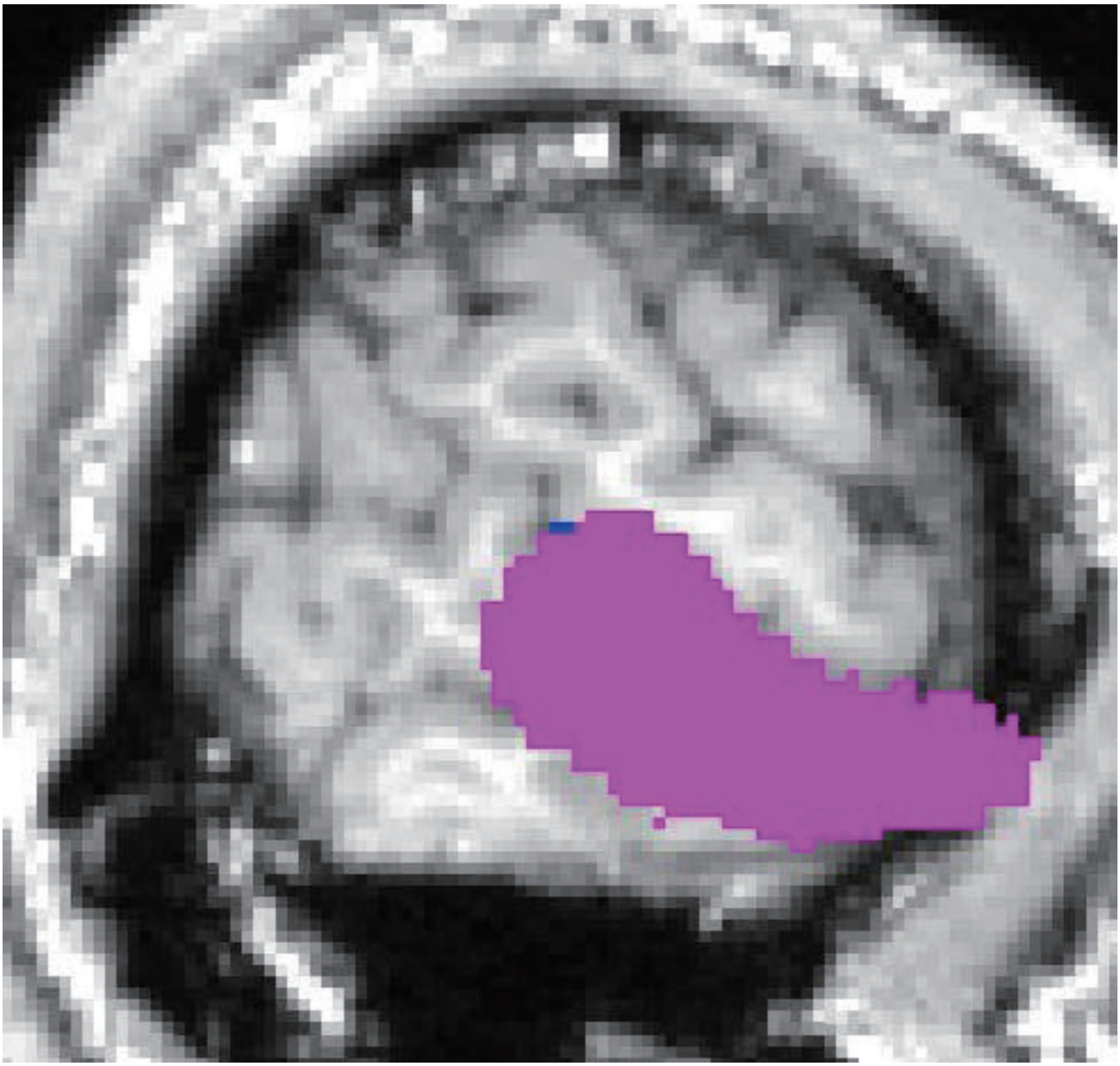

Supplementary Fig. 1(c)

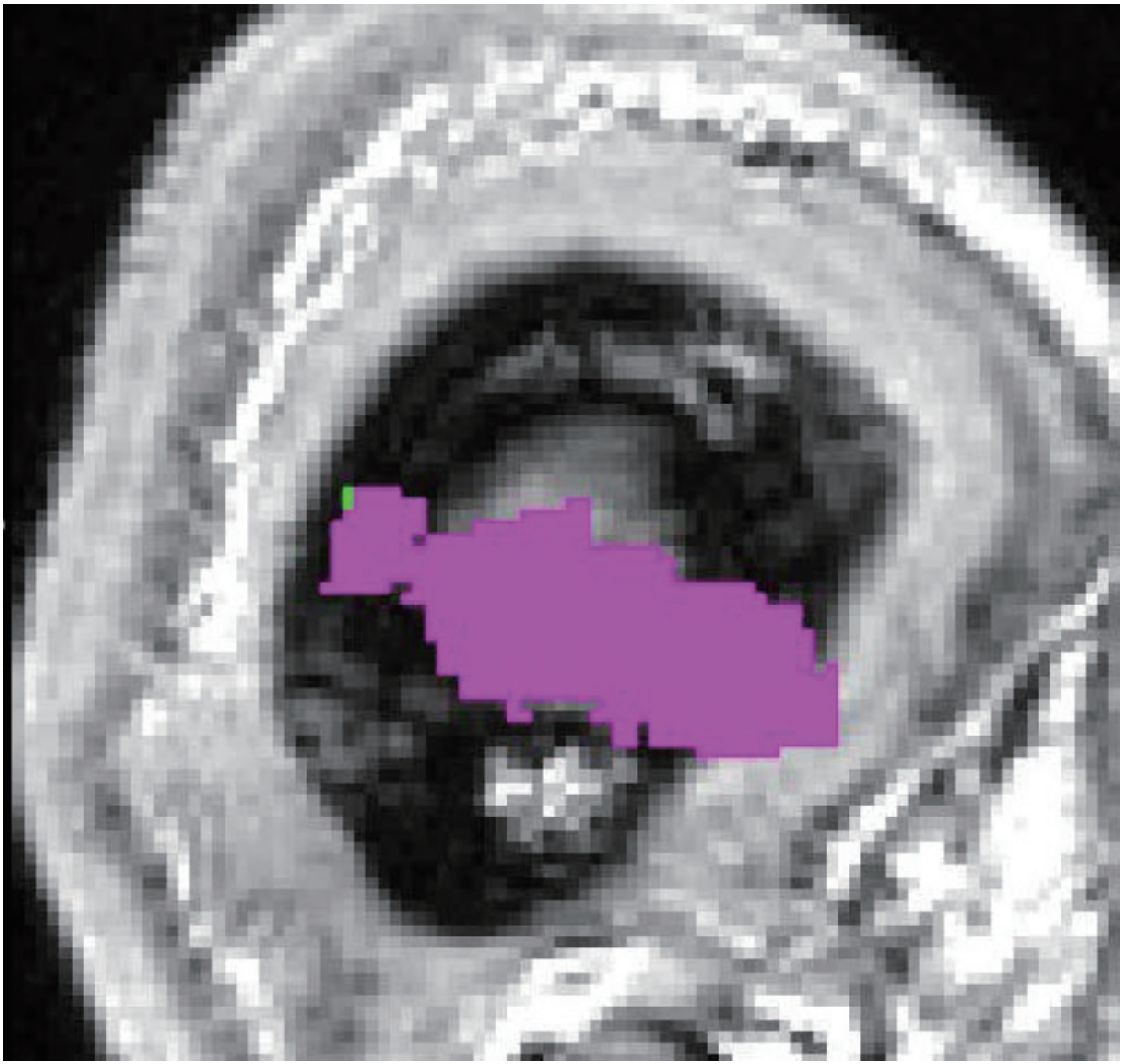

Supplementary Fig. 1(d)

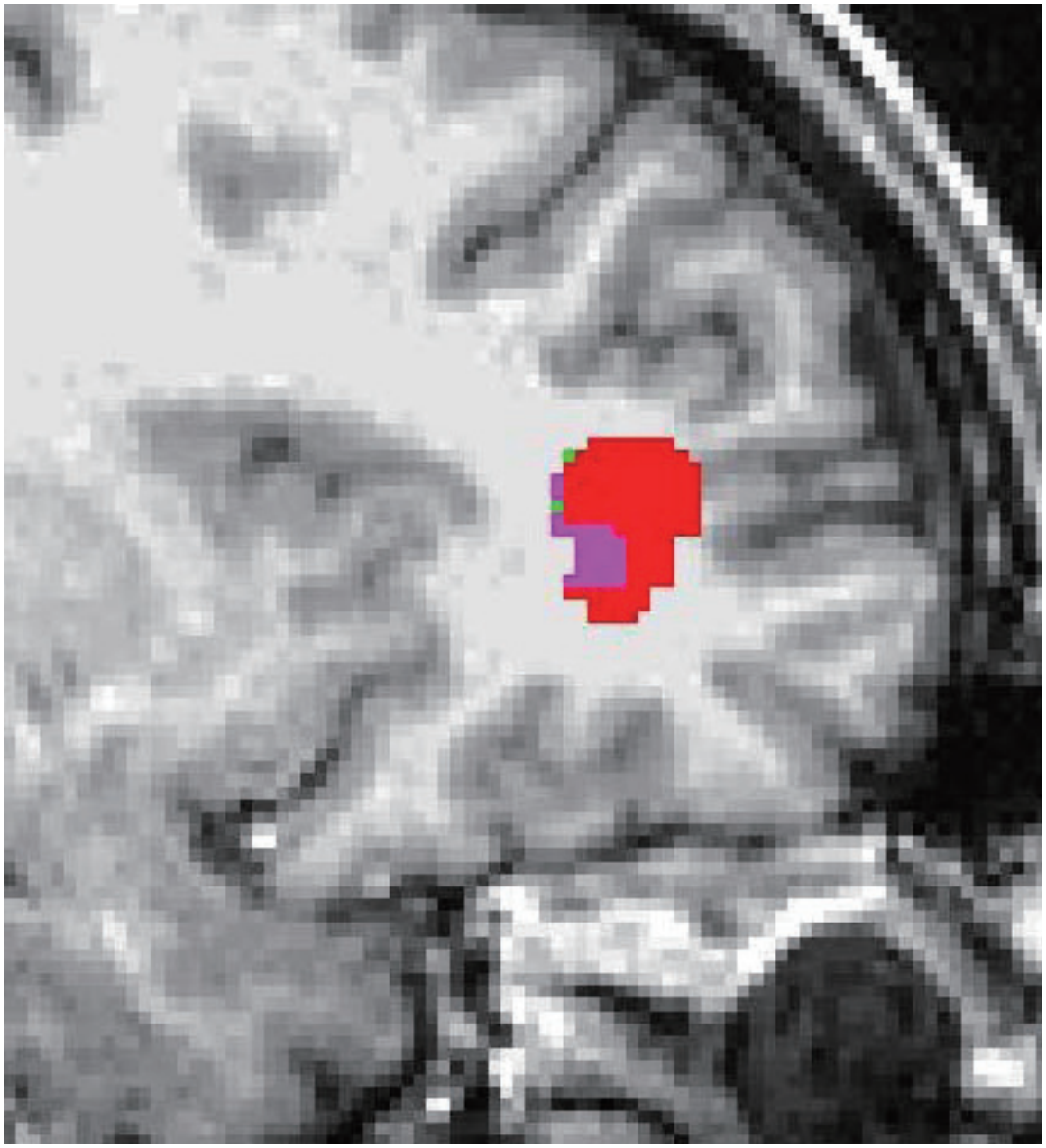

Supplementary Fig. 2

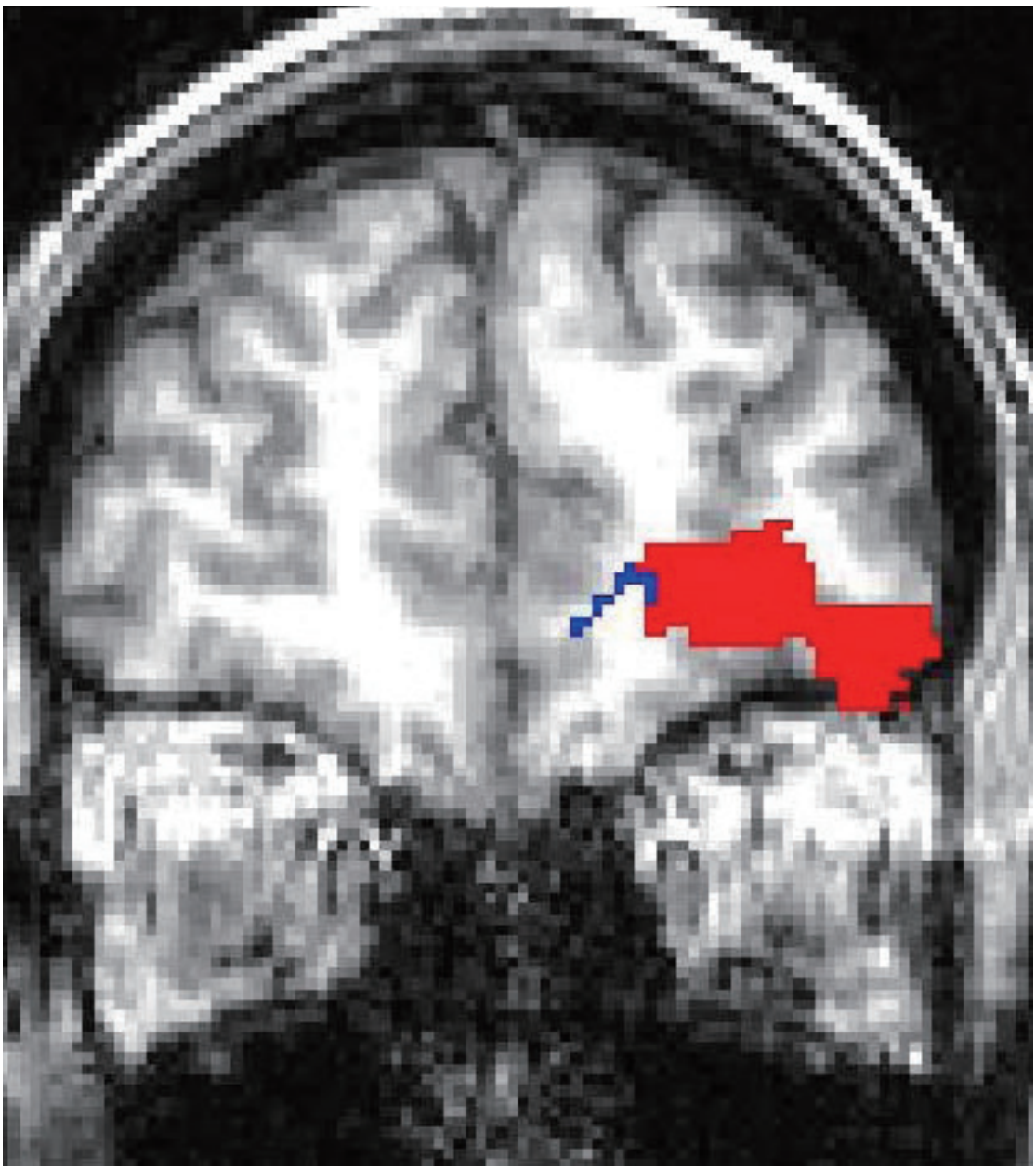

Supplementary Fig. 3(a)

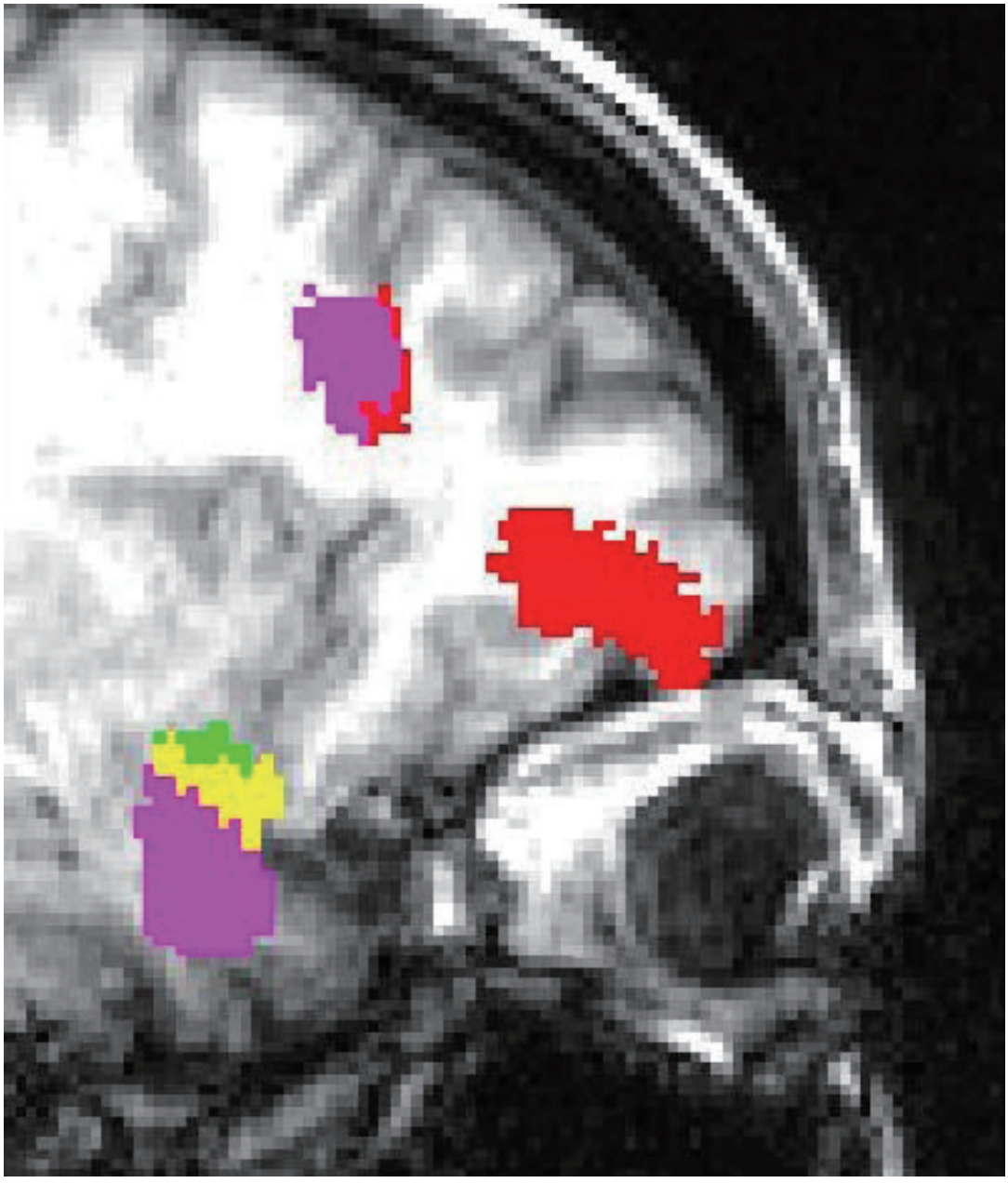

Supplementary Fig. 3(b)

Supplementary Fig. 4